ELSEVIER

Journal of Alloys and Compounds 279 (1998) 60–65

Journal of ALLOYS AND COMPOUNDS

A plasma kinetics model: analysis of wall loss reactions in dry etching of silicon dioxide

Kazutami Tago*, Hideyuki Kazumi, Kinya Kobayashi

Hitachi Research Laboratory, Hitachi, Ltd. 7-1-1 Omika-cho, Hitachi-shi, Ibaraki-ken 3 19-12, Japan

Abstract

Computational models for gas-phase chemical reactions in plasmas and for sticking reactions on metallic Al walls have been developed and applied to the plasma chemistry of dry etching of silicon dioxide. Dissociation paths and threshold energies of gases are determined by using an ab initio density functional molecular orbital method, and dissociation cross sections are approximated. The electron energy distribution function is determined by using a particle-in-cell model with the Monte Carlo collision method, and dissociation reaction rates are determined. Plasma densities, electron temperatures. and radical densities are calculated by a kinetic model which consists of the fluid equations for plasmas and rate equations for radicals. The model effectiveness was confirmed by results comparison for the Ar discharge in an radio-frequency device. The chemical compositions of the dry etching plasmas have been investigated for C_4F_8. Calculated electron temperatures and densities agree with experimental results within factors of three. Correlations could be found between the composition of radicals in the plasma and the etch selectivities in C_4F_8. Adsorption potentials of fluorocarbon radicals on Al (III) surface clusters have been calculated by using molecular orbital method, and sticking coefficients are estimated. Sticking coefficient of fluorine atom is the largest and decrease in order of F, C, CF, H, CF_2, and CF_3. Effects of hypervalence bonding at Al surface are discussed. Phenomena [1] of no film depositions in CF_4 RF plasma and film depositions in RF plasma of CF_4 mixed with H_2 were explained by hypervalence reactions of Al.

Keywords: Plasma chemistry; Composition; Surface reaction

1. Introduction

In developing the next generation of ultra large scale integration (ULSI) chips, aspect ratios of holes and trenches to be etched are increasing. In particular, the etching of contact holes through silicon dioxide layers to polycrystalline silicon or silicon nitride is becoming an important process. Fluorocarbon gases such as CHF_3, CH_2F_2 and C_4F_8 are used to obtain high etch selectivity of the SiO_2 film over a silicon underlayer.

In larger aspect ratios, more detailed understandings of etching mechanisms are needed, since larger costs are required to develop ULSI processes and processing devices. However, large unknown parts exist in mechanisms of silicon dioxide dry etching, as it is difficult to identify elementary processes of plasma generation and surface reactions experimentally and to measure composition of plasma and reaction products. We have used a computer simulation approach to obtain a better understanding of etching mechanisms.

A computational model has been developed and used to treat radical composition in plasmas, and chemical reactions on processing chamber walls have been analyzed. An ab initio density-functional molecular orbital method has been used to determine the products and threshold energies of dissociation reactions, and dissociation cross sections are estimated approximately. Electron energy distribution functions (EEDFs) in plasmas have been calculated by a particle kinetics model with Monte Carlo collisions. Dissociation rates are determined as a function of the electron temperature. Then, densities of radicals are calculated by plasma fluid kinetics model and reaction rate model. This model has been applied to the gas phase reactions in C_4F_8 plasma. Surface sticking reactions on Al wall have been analyzed with the ab initio density-functional molecular orbital method. Phenomena of no film depositions in CF_4 RF plasma and film depositions in RE plasma of CF_4 mixed with H_2 have been discussed.

2. Model

It is natural to calculate radical composition from the data of cross sections $\sigma^k(E)$'s of dissociation reactions of a

*Corresponding author.

0925-8388/98/$19.00
PII: S0925-8388(98)00612-4

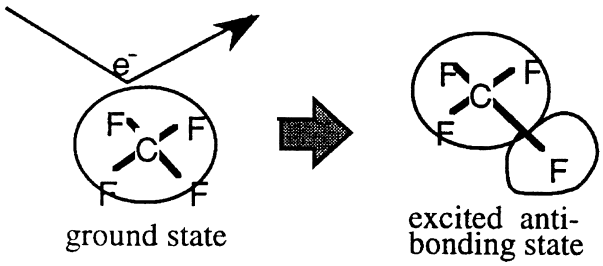

Fig. 1. Excitation to a dissociative orbital by electron impact.

molecule by an electron impact and EEDFs, as effects of electron temperatures and differences of plasma sources can be taken into account. However, $\sigma^k(E)$'s have not been measured for most of fluorocarbon gases. In our work [2], $\sigma^k(E)$'s were approximated by using experimental data and the ab initio density functional molecular orbital method, ESPAC-DF [3,4] with the local spin density approximation. Threshold energies of dissociations can be estimated from the difference between energies of the highest occupied orbital and excited anti-bonding orbitals of a molecule (Fig. 1). Dissociation reaction paths were read from the bond orders of excited anti-bonding orbitals. The calculated threshold energies for the lowest neutral and ionic dissociations agree with the experiments [5] within 15% for CF_4, SiH_4, CH_4, and Si_2H_6 as shown in Table 1. Dissociation paths and threshold energies E^k_{th} for C_4F_8 are shown in Table 2. Dissociation paths and E^k_{th} of neutral and ionic dissociation were estimated for fragments of C_4F_8 similarly.

Our approximation method for $\sigma^k(E)$'s are briefly shown. Each $\sigma^k(E)$ from an excited anti-bonding orbital was assumed to be a function with the equal maximum height and was made from an estimated total cross section by a factor-multiplication and energy-shift, as no information of $\sigma^k(E)$'s for each dissociation path can be available. The shape of each $\sigma^k(E)$ was assumed as a parabolic function considering the shape of the dissociative cross section of CF_4 [5]. The total dissociative cross section $a(E)$ for a molecule was written as follows:

$$a(E) = \sum_k \sigma^k(E)$$

$$= \sum_k \sigma_0(E - E^k_{th})(E^k_b E)/\{(E^k_m - E^k_{th})(E^k_b - E^k_m)\},$$

where, $\sigma_0 = \sigma_m$/(number of dissociation paths), $E^k_b = 2E^k_m - E^k_{th}$, $E^k_m = E^0_m$, σ_m is peak value of the total dissociative cross section estimated from CF_4 [5], and E^0_m is the energy at the peak of the total dissociative cross section of CF_4 [5]. As E^0_m for CF_4 is about 100 eV [5], E^k_m for C_4F_8 was set as 100 eV. The peak value σ_m for C_4F_8 was set by multiplying that of CF_4 by (number of bonds of C_4F_8)/(number of bonds of CF_4). Dissociative cross sections for C_4F_8 are shown in Fig. 2. Dissociative cross sections for fragments and ionization cross sections were estimated by a similar procedure. The total dissociative cross section for CF_4 estimated with the above formula has the similar shape as that of [5]. Although we do not have a means with which accuracy of cross sections for C_4F_8 and its fragments can be discussed, tendencies of composition changes may be discussed.

The rate coefficient is expressed as

$$k = A \int \sigma(E) E^{1/2} f(E)\, dE \quad (1)$$

where $f(E)$ is electron energy distribution function (EEDF) and A is normalization factor for $f(E)$. The $f(E)$ is estimated by a plasma kinetic method using particle model [6,7], with collisions treated by Monte Carlo method. To

Table 1
Dissociation threshold energies

Molecule	Dissociation products	Threshold calc.	Energy (eV) experiment [3]
CF_4	CF_3+F	10.7	12.5
	$CF_3^+ + F$	17.0	16.2
CH_4	CH_3+H	10.1	10.0
SiH_4	SiH_2+H_2	8.6	9.0
Si_2H_6	SiH_3+SiH_3	5.5	6.0

Table 2
Calculated dissociation products and threshold energies for C_4F_8

Products	Threshold energies (eV)	Products	Threshold energies (eV)
C_4F_7+F	5.5	$4CF_2$	11.7
C_4F_7+F	7.2	$C_2F_4+C_2F_4^+ + e^-$	13.9
$C_2F_4+C_2F_4$	9.0	$C_2F_4+C_2F_4^+ + e^-$	15.2
C_4F_7+F	9.7	C_4F_7+F	16.0
$C_4F_6+F_2$		$C_2F_4+C_2F_4^+ + e^-$	18.3
$C_2F_4+C_2F_4$	9.8	$C_2F_4+C_2F_4^+ + e^-$	21.3
$C_2F_4+C_2F_3+F$		$C_2F_4+C_2F_4^+ + e^-$	22.0
C_4F_7+F		$3CF_2+CF_2^+ + e^-$	25.3
$C_2F_4+C_2F_4$	10.5		

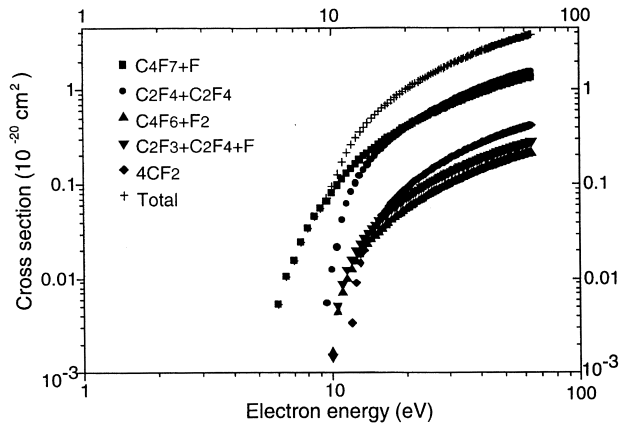

Fig. 2. Dissociative cross sections for C_4F_8.

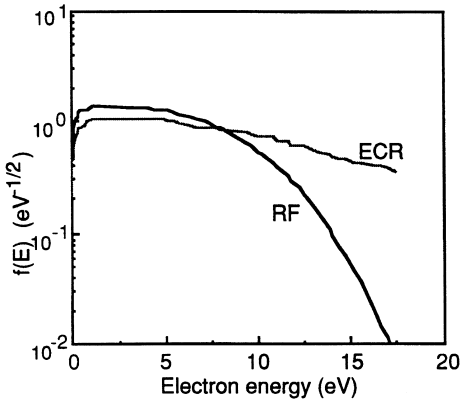

Fig. 3. Electron energy distribution functions in Ar discharge for RF and ECR devices.

treat interactions between particles and electromagnetic fields, particle-in-cell (PLC) model is used. Space dimensions of the particles are 1 in positions and 3 in velocities. EEDF is calculated by average operation for all the particles. Fig. 3 shows EEDFs in Ar discharge for electron cyclotron resonance (ECR) device with typical conditions of 1 mTorr gas pressure and 1 W cm^{-2} microwave power and for radio frequency (RF) device with 0.3 Torr, 1 kV, and 2 cm plate distance. The ECR curve has a high energy a tail, which is missing in the RF curve. The electron energies for the space average are about 7 eV for ECR, and 4.5 eV for the RE device.

Then, dissociation reaction rate coefficient (DRRC) is determined as function of the electron temperature for each dissociation path. Fig. 4 shows DRRCs in Ar discharge for RF device. DRRCs of large threshold energies, such as for the excitation to a metastable state Ar* (11.56 eV) and the direct ionization (15.70 eV), change sharply with electron temperature. DRRCs for small threshold energy is nearly constant against electron temperature. DRRCs for C_4F_8, their fragments, and rare gases have been determined.

To obtain plasma and radical densities and electron temperatures, plasma kinetics are modeled by a set of one dimensional fluid equations that consists of continuity and momentum conservation equations for ions and energy conservation and quasi-neutrality equations for electrons, connected with the Poisson equation for electrostatic plasma fields.

Densities of radicals arc calculated on the basis of diffusion equations including dissociation reactions by electron impact and chemical reactions between radicals. Basic diffusion equations are defined as,

$$\partial n_1/\partial t = (\sum k_{lje} n_e n_j - \sum k_{jle} n_e n_l) + (\sum k_{ljk} n_j n_k - \sum k_{kij} n_l n_j) + \nabla(-D\nabla n_l) - S_w + S \quad (2)$$

Here, n_e, n_1 and D are electron density, neutral density of the lth species and diffusion coefficient, respectively. The k_{ije}, k_{ijk} are the rate coefficients for generating ith neutral species through dissociation of the jth neutrals and through neutral–neutral chemical reactions respectively. The fourth term S_w is exhaust by pump system which changes with time, and is introduced to account for the effect that total gas pressure is usually kept constant during the operation of a device. S denotes gas input. The effects of surface reactions such as sticking and gasification, which really influence the composition of radicals, especially, for a narrow gap RF device, are not included in the present model, due to lack of knowledge in surface reactions. Individual treatments of radical reactions at the walls are shown in applications of the next section.

To understand sticking reactions on Al walls, energetics between fluorocarbon radical fragments and Al clusters are analyzed by using ESPAC-DF with the generalized gradient approximation [8,9] with a Slater-type basis set of the quality of double zeta and a polarization function. Sticking coefficients on the Al wall are roughly estimated from adsorption potential curves.

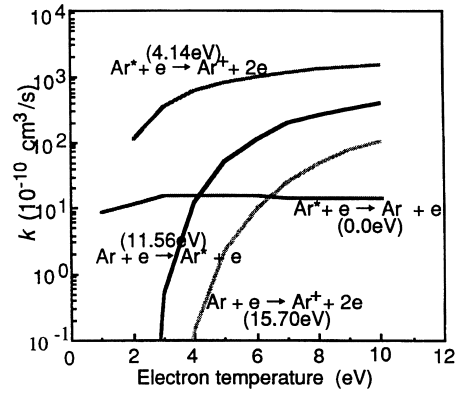

Fig. 4. Rate coefficients of electron impact reactions for Ar discharge in RF device.

3. Results and discussions

3.1. Ar discharge

The plasma fluid kinetic model was applied to Ar discharge in an RF device to check its effectiveness, since cross sections for Ar are well known. In an Ar discharge there is a large amount of metastable Ar* which plays an important role in ionization especially in RF devices. Ar* is assumed to change to Ar at the walls. Time-averaged densities of Ar* and Ar+ are shown in Fig. 5, which agree with the experimental values [10] within factors of one and three, respectively. The densities of Ar* and Ar^+ are 2.8×10^{18} m^{-3}, and 2.5×10^{17} m^{-3} respectively. It is found out that in the ECR device the ratios of ions to

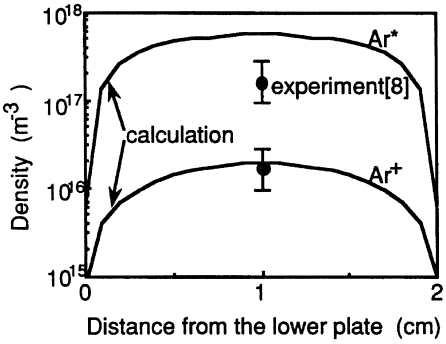

Fig. 5. Calculated and experimental plasma densities [8] for Ar discharge.

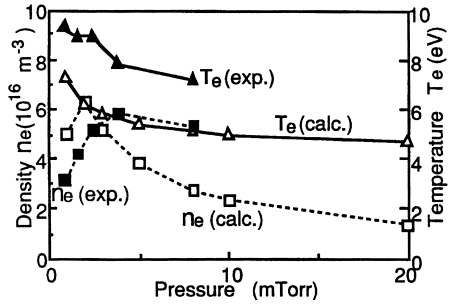

Fig. 7. Electron temperature and density in C_4F_8.

neutral species Ar^+/Ar* and metastable (radicals) to gas Ar*/Ar are larger than those in the RE device.

3.2. The composition of radicals in C_4F_8 plasma

The calculated densities of radicals and ions for an ECR device are shown in Fig. 6. Effects of radical sticking to reactor walls on composition were ignored as ion bombardments are weak and knowledge of surface reactions are unavailable. The lower the gas pressure is, the more dissociation proceeds due to the increase of electron temperature and density. At 2 mTorr, C and CF densities increase to the levels of C_2F_4 and CF_2 densities and the relative ratio of F decreases.

A comparison of calculated and experimental plasma characteristics is shown in Fig. 7. The calculated results qualitatively agree with the experiments within factor of three. However, the calculated T_e is so low that the pressure giving the maximum plasma density shifts to a lower value compared to the experimental result. This difference may come from the uncertainties of the magnitudes of various cross-sections of neutral and ionic fragments.

It is well known that fluorocarbon radicals generated in a plasma impinge and deposit on the wafer surface. This fluorocarbon film, formed on polycrystalline silicon or silicon nitride, protects the surface from impinging ions and produces high etch selectivity. It has been reported that etch selectivity over Si and etched shape of contact holes depend on film characteristics, i.e. C/F ratio and film thickness [11]. The correlation between the calculated composition of the radicals and plasma etch characteristics has been considered. The C/F ratio in fluorocarbon films is estimated from the gas phase composition assuming sticking coefficients (C and $C_xF_y = 10^{-2}$; $F = 10^{-3}$). The dependence of the C/F ratio on pressure is shown in Fig. 8. Lowering gas pressure, C/F increases with the degree of dissociation (increase in ratios of CF and C radicals). The etch selectivity of SiO_2 over Si_3N_4, also shown in Fig. 8, has the same dependence as C/F on gas pressure. Etch selectivities of SiO_2 over poly-Si and resist show the same dependencies on gas pressure.

It seems suitable to operate the device at low pressure (high n_e and T_e) and low flow rate (long residence time) in order to obtain high selectivity of SiO_2 over Si_3N_4.

3.3. Radical sticking onto Al (III) surfaces

Although it is important to know sticking coefficients on to deposited fluorocarbon films, especially, for a RF device, we treat sticking reactions to surfaces before film deposition. ESPAC-DF was used with the generalized gradient approximation (GGA) [8,9] to obtain reaction energies. Fig. 9 shows an adsorbed structure of CF_3 on to Al(111) surface. Similar calculations were done for CF_2, CF, C, F and H. On-top site gives the largest adsorption

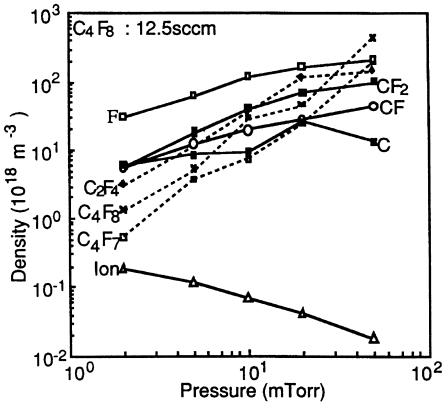

Fig. 6. Dependence of radical densities on pressure in C_4F_8.

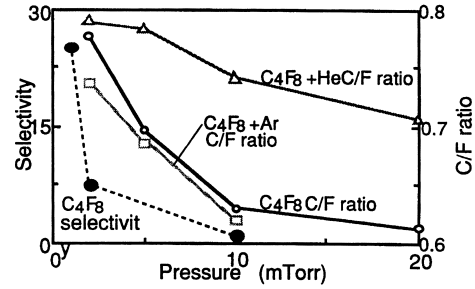

Fig. 8. Estimated C/F ratio and selectivity of SiO_2 over Si_3N_4.

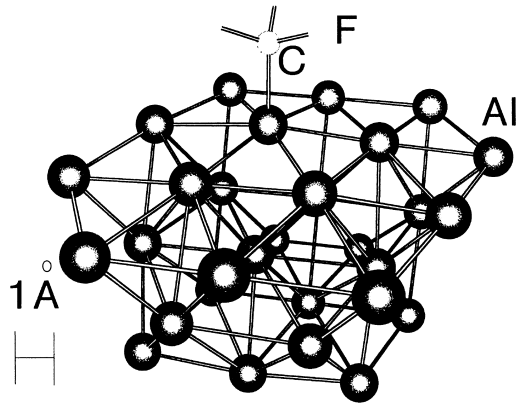

Fig. 9. Adsorbed structure of CF_3 on Al(III) surface atomic cluster.

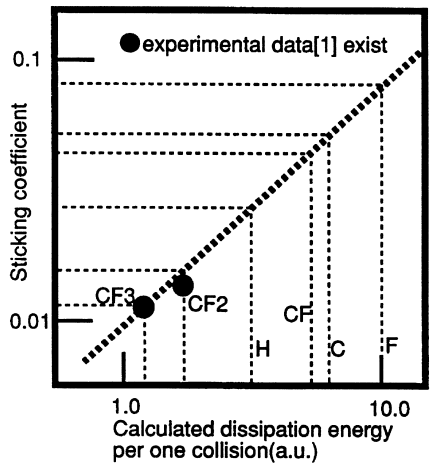

Fig. 11. Calculated sticking coefficients of radicals on Al surface.

energy for CF_3, F and H, bridge-site for CF_2, and hollow-site for CF and C, respectively.

Fig. 10 shows adsorption potential curves for CF_3, CF_2, and CF. The potential ranges of them decrease in order of CF, CF_2, and CF_3. The potential depths, from deepest to shallowest, are in the order: CF, CF_3, and CF_2. CF seems to have the largest sticking coefficient. From the theory of collision processes to the surface [12,13], sticking coefficient is proportional to the energy loss of the fragment at the surface and the energy loss is proportional to (surface friction) (particle stay time) (particle kinetic energy). As surface friction is proportional to (total integral of self-correlation function of electron density fluctuations)/(particle mass), assuming the integral is a constant for the same surface, energy losses, i.e., sticking coefficients, are proportional to (potential range) (potential depth/particle mass)$^{1/2}$. From the adsorption potentials, sticking coefficients are estimated as shown in Fig. 11 by calibrating with experimental surface loss coefficient of CF_3 [1]. Although the experiment [1] does not treat the pure metal surface, similar mechanism of sticking was assumed. The sticking coefficients decrease in order of F, C, CF, H, CF_2, and CF_3. F has the largest sticking coefficient.

In the experimental condition [1], as RF plasma weakly decomposes CF_4, the radicals F, CF_3, and CF_2 may be dominant. Due to large sticking coefficient of F, the surface of Al wall may be covered by Al–F bonding and no fluorocarbon film depositions occur. However, when 10% H_2 gas is mixed in CF_4, deposition starts. The phenomena can be explained from hypervalence reactions of Al in Table 3 calculated with ESPAC-DF. Al usually has three valence bonds but can bind with the fourth atom of large binding energy such as F. This hypervalence bonding is weak for bonding with CF_3 or H. And hypervalence bonding F (HBF) can be easily removed by radicals such as AlF_2, H and CF_x. From these results, Al surface can contain a lot of HBFs for CF_4 RF plasma and areas of F deficiency created by ion bombardments may be repaired to the usual full valence bonding state by nearby HBFs. Then, no film depositions can occur. However, when 10% H_2 gas is mixed, a large channel of removing HBFs by H radicals opens and HBFs may become insufficient to repair active areas created by ion bombardments. Then. fluorocarbon film deposition may start. To estimate deposition rates and composition of film, sticking coefficients on fluorocarbon films and effects of ion bombardments should be understood quantitatively.

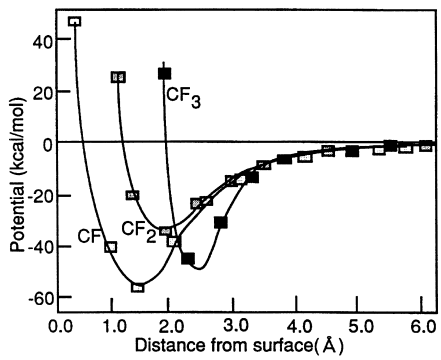

Fig. 10. Adsorption potentials of CF_3, CF_2, and CF on Al atomic cluster.

Table 3
Calculated energies of hyper-valence reactions of Al with the generalized gradient approximations

Reactants	Products	Generated energies (eV)
AlF_3+F	AlF_4	1.5
AlF_3+F	AlF_4	0.7
AlF_4+AlF_2	$2AlF_3$	5.0
AlF_4+H	AlF_3+HF	4.5
AlF_4+CF_3	AlF_3+CF_4	4.0
AlF_3+H	F_3AlH	0.18
AlF_3+H	F_3AlH[a]	0.15 [a]
AlF_3+CF_3	F_3AlCF_3	0.28
AlF_3+CF_3	F_3AlCF_3 [a]	0.22 [a]

[a] Sticking reaction with rigid AlF_3.

4. Conclusion

A computational model for chemical reactions in plasmas has been developed. An ab initio molecular orbital method was used to determine the products and threshold energies of dissociation reactions. Plasma characteristics were calculated by the plasma chemical kinetic model which consisted of particle model with Monte Carlo collisions, fluid equations for a plasma, and rate equations for radicals. This model was applied to C_4F_8 plasma. Calculated plasma electron temperatures and densities agreed with experimental results within factors of three. The lower the gas pressure was, the greater the degree of dissociation which occurred and the estimated C/F ratio increased. Sticking coefficients of radicals on to Al (III) surface were estimated by using ESPAC-DF. They decrease in order of F, C, CF, H, CF_2, and CF_3. Phenomena [1] of no film depositions in CF_4 RF plasma and film depositions in RF plasma of CF_4 mixed with H_2 were explained by hypervalence reactions of Al.

References

[1] Y. Hikosaka, H. Toyoda, H. Sugai, Jpn. J. Appl. Phys. 32 (1993) L690.
[2] H. Kazumi, K. Tago, Jpn. J. Appl. Phys. 34 (1995) 2125.
[3] K. Kobayashi, K. Tago, H. Kumahora, N. Kurita, in: M. Doyama et al. (Eds.), Computer Aided Innovation of New Materials II, Elsevier Science Publishers, B.V., 1993, p. 165.
[4] K. Kobayashi, N. Kurita, H. Kumahora, K. Tago, Phys. Rev. B45 (1992) 13690.
[5] M. Hayashi, in: Swarm Studies and Inelastic Electron Molecule Collisions, Springer, New York, 1987, p. 167.
[6] H. Kazumi, T. Tetsuka, K. Yoshioka, Proc. 9th Symp. Plasma Processing, 225 (1992).
[7] The Extended Abstracts of 53rd Autumn Meeting of the Jpn. Soc. Appl. Phys. 19a-A-10 (1992).
[8] J.P. Perdew, Y. Wang, Phys. Rev. B33 (1986) 8800.
[9] J.P. Perdew, Y. Wang, Phys. Rev. B40 (1989) 3399.
[10] K.E. Greenberg, G.A. Hebner, J. Appl. Phys. 73(8) (1993) 126.
[11] Y. Miyakawa et al., Proc. 15th Symp. on Dry Process, Tokyo November, 91 (1993).
[12] H. Muller, W. Brenig, Z. Phys. B34 (1979) 165.
[13] M. Tsukada, in Introduction to Surface Physics in Japanese, University of Tokyo Press, Tokyo, 1989, p. 144.